Available online at www.sciencedirect.com
ScienceDirect
Geochimica et Cosmochimica Acta 70 (2006) 5802–5813
Geochimica
www.elsevier.com/locate/gca

Calcite dissolution kinetics in Na–Ca–Mg–Cl brines

Dwight K. Gledhill *, John W. Morse

Department of Oceanography, Texas A&M University, MS 3146, College Station, TX 77843, USA

Received 29 August 2005; accepted in revised form 29 March 2006

Abstract

Sedimentary basins can contain close to 20% by volume of pore fluids commonly classified as brines. These fluids can become undersaturated with respect to calcite as a result of migration, dispersive mixing, or anthropogenic injection of CO_2. This study measured calcite dissolution rates in geologically relevant Na–Ca–Mg–Cl synthetic brines (50–200 g L^{-1} TDS). The dissolution rate dependency on brine composition, pCO_2 (0.1–1 bar), and temperature (25.0–82.5 °C) was modeled using the empirical rate equation

$$R = k(1 - \Omega)^n$$

where R is the rate, k and n are empirical fitting terms and $1 - \Omega$ the degree of disequilibrium with respect to calcite. When Ω is defined relative to an apparent steady-state solubility, n can be assumed first-order over the range of Ω investigated ($\Omega = 0.2$–1.0). Rates increased with increasing pCO_2 as did its sensitivity to increased brine total dissolved salt (TDS) concentration. At 0.1 bar, rates were nearly independent of the TDS ($k = 13.0 \pm 2.0 \times 10^{-3}$ mol m^{-1} h^{-1}). However, at higher CO_2 partial pressures, rates became composition dependent and the rate constant, k, was shown to be a function of temperature, pCO_2, ionic strength and calcium and magnesium activity. The rate constant (k) can be estimated from a multiple regression (MR) model of the form

$$k = \beta_0 + \beta_1(t) + \beta_2(\mathrm{pCO_2}) + \beta_3(I) + \beta_4(a_{\mathrm{Ca^{2+}}}) + \beta_5\left(a_{\mathrm{Mg^{2+}}}\right).$$

A relatively high activation energy ($E_a = 20$ kJ mol^{-1}) was measured, along with a stirring rate independence suggesting that the dissolution is dominated by surface-controlled processes at $\Omega > 0.2$ in these calcium-rich brines. The addition of 1 g L^{-1} SO_4^{2-} resulted in a rate inhibition that was highly sensitive to increasing concentrations of calcium and magnesium. Consequently, even though sulfate concentrations in subsurface formation waters are generally less than that in seawater, at TDS concentrations greater than 200 g L^{-1}, its effect on the rate may be of similar magnitude. These findings provide an opportunity to improve reaction-transport models in carbonate-bearing saline reservoirs, where pCO_2 is >0.1 atm (pH < ~6.5), by adding considerably more realistic reaction kinetics. This will be of considerable importance in modeling of CO_2 sequestration in carbonate-hosted reservoirs.

1. Introduction

Pore waters contained in sedimentary rocks can range in salinity by approximately five orders of magnitude (Hanor, 1994a), from dilute meteoric waters, to waters with greater than 600 g L^{-1} of dissolved salts (Case, 1945). There is growing interest in the geochemistry of these formation waters as reservoirs are being developed as possible repositories for waste gases and fluids. Mineral–brine–waste interactions will influence processes affecting the post-injection development of secondary porosity, reservoir permeability and mass transport in the subsurface.

Carbonate minerals constitute ~20% of Phanerozoic sedimentary rock, and at least 60% of the world's know petroleum reserves occur in carbonate reservoirs (Morse and Mackenzie, 1990). Because calcite is a common reactive mineral, its precipitation and dissolution are of great importance in the creation and destruction of secondary porosity in the subsurface.

* Corresponding author. Fax: +1 301 713 3136.
E-mail address: dwight.gledhill@NOAA.gov (D.K. Gledhill).

0016-7037/$ - see front matter © 2006 Elsevier Inc. All rights reserved.
doi:10.1016/j.gca.2006.03.024

A large number of investigators have examined the influences of 'foreign' ions, temperature, CO_2 partial pressure and other variables on calcite dissolution rates (see reviews of Plummer et al., 1979; Sjöberg and Rickard, 1983; Morse, 1983; Morse and Arvidson, 2002). Previous investigations sought to understand the behavior of calcite in solutions with ionic strengths that did not generally exceed that of seawater. Calcite reaction kinetics in concentrated solutions, typical of the subsurface, have received relatively little attention. Although a few recent studies included precipitation rate measurements in higher salinity waters (Zhang and Dawe, 1998; Zuddas and Mucci, 1998), fewer have directly addressed the dissolution kinetics of carbonate minerals in complex high ionic strength solutions (e.g., Pokrovsky et al., 2005). Investigation of carbonate mineral dissolution as a function of saturation state requires accurate calculations of the carbonic acid system species distributions. Whereas determination of the activities of these species in high ionic strength solutions continues to be problematic, investigations of the solubility of calcite coupled with the Pitzer parameterizations of the carbonic acid system in synthetic brines (He and Morse, 1993) have made such calculations more reliable.

Although the composition of subsurface formation waters vary considerably, fortunately this variably is not entirely random as Hanor (1994b) demonstrated. Instead, much of the variability can be explained by mineral–brine equilibration considerations. This constrains somewhat the concentration of the major dissolved species as a function of TDS. Using this relation, we have determined the dissolution kinetics of calcite in saline waters with compositions approximating those in Northern Hemisphere reservoirs. The results have important applications to predictive chemical process models in carbonate cemented reservoirs and for carbon sequestration strategies.

2. Experimental

2.1. Materials

2.1.1. Aqueous solutions

Synthetic Na–Ca–Mg–Cl brines were prepared gravimetrically on the molal scale (m) from separate concentrated stock solutions of A.C.S. reagent grade NaCl, $CaCl_2{\cdot}2H_2O$ and $MgCl_2{\cdot}6H_2O$. Phosphate measurements of the concentrated stock solutions were made according to the methods of Murphy and Riley (1962) and in all cases found to be below detection (<1 μM). Three 'model' brines were investigated containing 50, 125 and 200 g L^{-1} total dissolved solids (TDS). A multivariate approach was used such that calcium, magnesium and ionic strength were co-varied as a function of TDS according to Hanor (1994b). Modifications to each of these 'model' brines were then made where the specific effects of a given variable were explored. The initial salt concentrations were verified by analytical determination of calcium, total hardness and chloride concentrations.

Brines were reacted with crushed rhombic Iceland spar calcite obtained from Ward's Scientific Inc. A 63–125 μm size fraction was collected by wet sieving. To relieve surface strain and to clean the grains of ultra-fine particles which can enhance solubility, the crushed material was sonicated in methanol for one hour, re-sieved, briefly washed with MilliQ® (18.1 μΩ) water followed by freeze drying. Specific surface area was estimated to be 0.02 m^2 g^{-1} from a geometric determination using scanning electron micrograph (SEM) imaging. The mineralogy was verified by powder X-ray diffraction as being >99% calcite.

2.1.2. Solution chemistry

Solution concentrations of Cl^- were determined by $AgNO_3$ titration (±1.5%) using an Accumet silver ion selective electrode interfaced with a computer via an Orion 720A potentiometer. Calcium was analyzed by EGTA titration with calcium indicator Cal/Ver II® and Mg^{2+} concentrations were determined by EDTA titration with Erichrome Black (EBT). Endpoint detection was facilitated using a Brinkmann PC 800 colorimeter interfaced with a Brinkmann 682 titroprocessor. Precision was within 2% in most cases. The concentration of Na^+ was calculated from charge balance.

Total carbon dioxide (TCO_2) was determined according to the method of Dickson and Goyet (1994) with a UIC Inc. Model 5011 CO_2 coulometer. Precision ranged from 3.7% at low concentrations (i.e., <0.003 m) to better than ±0.3% at high concentrations (i.e., >0.03 m). Total alkalinity (TA) was determined by a Gran-type titration (Gran, 1952) using a Metrohm 655 Dosimat and an Orion 720 A pH meter interfaced with a computer. Apparent sample pH was measured using a Corning Inc. semi-micro combination pH electrode calibrated using NIST-traceable 4 and 7 buffers. Computer software was used to evaluate the inflection point. An HCl titrant and solutions of primary standard Na_2CO_3 were prepared in NaCl solutions at ionic strengths specific to each of the brines. The Na_2CO_3 standards were prepared gravimetrically under a nitrogen environment and their concentrations verified by TCO_2 coulometeric measurement. Four point calibration curves were made using weighted standards versus the volume at which the inflection point occurred. Precision was better than 0.1 meq kg^{-1}. Titrations were conducted at 25 ± 0.1 °C in a water-jacketed open cell into which CO_2 was continuously bubbled. Bubbling of CO_2 into the cell served to facilitate gas exchange and prevent the solution from becoming oversaturated with respect to $CaCO_3$ mineral phases as a result of degassing prior to the addition of the HCl titrant.

The solution pH was measured using a Ross® H^+ selective electrode referenced to a Single Refex® solid-state reference electrode. The Refex® reference electrode uses an ionically conductive hard-non-porous salt loaded polymeric matrix. The matrix acts as an immobilized electrolyte thus avoiding a porous liquid-junction. Calibration of the electrodes to 'Pitzer scale' pH was performed according

to the methods of Gledhill and Morse (2004). Briefly, the initial and final pH of the brine is calculated by coupling TA and TCO_2 using the Pitzer equation-based program EQPITZER (He and Morse, 1993). The electrode response slope (S_x) can then be established using a two-point calibration from

$$S_x = \frac{E_f - E_i}{pH_i - pH_f} \quad (1)$$

where E is the emf and pH is the calculated 'Pitzer pH', initial (i) and final (f).

2.2. Dissolution reactor

An open system pH-free-drift method was employed in which the rate of $CaCO_3$ dissolution was determined by monitoring changes in solution pH as a function of time (Fig. 1). A 550 mL water-jacketed reaction vessel accommodated a gas feed, two electrodes, condenser/vent, temperature probe and sampling port. The solution was stirred at constant rate with a propeller shaft passed through the top of the reactor (Table 1). Temperature was held constant at (±0.1 °C) using a Neslab® constant-temperature bath and pCO_2 was maintained by bubbling with a humidified ultra high purity nitrogen–CO_2 gas mixture appropriate for the desired experimental conditions (Table 1). A mass-flow controller interfaced with a computer assured constant flow rate (2 L min^{-1}).

Common to open system free-drift experiments, if the initial rate of dissolution is too rapid, gas phase disequilibrium can occur in which there is an excess consumption of CO_2 relative to supply in the solution (e.g., Arakaki and Mucci, 1995). This can be prevented by: (1) conducting the dissolutions at high pCO_2 where appropriate; (2) reducing the available calcite surface area; (3) avoiding initiating the experiments at extreme degrees of disequilibrium. These experiments were conducted near 0.1 bar pCO_2 or greater and the calcite used exhibited a relatively low specific surface area. The low specific surface area also produced considerably slower initial rates allowing for significant amounts of calcite to be added (~4 g L^{-1}), thus minimizing the change in surface area during the experiments. Finally, a concentrated primary standard grade Na_2CO_3 solution was added to establish approximately 20% saturation with respect to calcite. These precautions resulted in little variation between initial and final pCO_2 values.

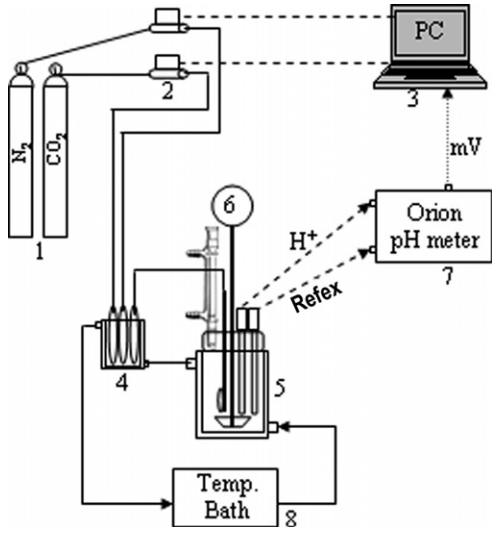

Fig. 1. Open system pH-free-drift batch reactor used to measure calcite dissolution rates in concentrated synthetic brines. The elements of the experimental setup are illustrated in the schematic: (1) high grade nitrogen and carbon dioxide gas; (2) dual MKS® Type 1479A mass-flow regulators; (3) computer; (4) gas humidifier; (5) batch reactor; (6) stir motor; (7) Orion® 720A pH meter; (8) Neslab® RTE-8DD circulating bath.

Prior to calcite addition, a 20 mL sample was drawn for initial solution analysis. The calcite was then allowed to react with the solution while changes in solution pH were monitored at 5 s intervals. Experiments were terminated typically after 5 h, at which point changes in solution chemistry were within the measurement precision. Triplicate 20 mL samples were drawn and filtered through a Millipore 0.45 μm syringe filter for final solution analysis. Calcite remaining in solution was collected by vacuum filtration and briefly rinsed with MilliQ® (18.1 μΩ) water. The filtered material was freeze dried and stored in a vacuum desiccator for later SEM imaging to confirm that there was no excessive alteration to the specific surface area.

3. Results

Table 1 reports measured salt concentrations prior to reaction with calcite along with the experimental conditions including gas mix ($X_{CO_2} = 1 - \frac{CO_2,\ L\ min^{-1}}{CO_2+N_2,\ L\ min^{-1}}$, where $CO_2 + N_2 = 2$ L min^{-1}), temperature (°C) and stir rate (revolutions per minute). Table 2 lists the CO_2-related parameters at the start of each experiment and the mean ($n = 3$) steady-state values following reaction with calcite. The electrode response yielded good agreement (90 ± 5%) with the ideal Nernst value even at high temperature. Although EQPITZER accurately modeled changes in TCO_2 relative to TA, with increasing calcium concentration the algorithm systematically overestimated calcite solubility (see Gledhill and Morse, in press, for a complete discussion). The pCO_2, calculated from TA and TCO_2, showed good agreement between initial and final values.

4. Discussion

4.1. Calculation of dissolution rate

The dissolution of 1 mol of calcite contributes 2 mol of TA, as given by the overall reaction,

$$CaCO_3 + CO_2 + H_2O \rightarrow Ca^{2+} + 2HCO_3^- \quad (2)$$

Thus, the dissolution rate can be defined from the time dependent rate of change in TA

Table 1
Initial solution concentration and experimental conditions

~TDS	Experiment	Ca^{2+}	Mg^{2+}	Na^{+}	Cl^{-}	SO_4^{2-}	I	X_{CO_2} [a]	°C	RPM
50	PCO2_01	0.039	0.0229	0.7390	0.8504	0.0000	0.9235	1.0	25.0	300
125	PCO2_02	0.157	0.0651	1.8210	2.2610	0.0000	2.4889	1.0	25.0	300
200	PCO2_03	0.347	0.1223	2.7310	3.6670	0.0000	4.1395	1.0	25.0	300
50	PCO2_04	0.039	0.0217	0.7351	0.8485	0.0000	0.9175	0.5	25.0	300
125	PCO2_05a	0.162	0.0677	1.8270	2.2830	0.0000	2.5169	0.5	25.0	300
125	PCO2_05b	0.154	0.0703	1.7660	2.2110	0.0000	2.4399	0.5	25.0	500
125	PCO2_05c	0.156	0.0656	1.6980	2.1360	0.0000	2.3611	0.5	25.0	700
200	PCO2_06	0.351	0.1234	2.7270	3.6740	0.0000	4.1501	0.5	25.0	300
50	PCO2_07	0.039	0.0228	0.7398	0.8592	0.0000	0.9247	0.1	25.0	300
125	PCO2_08	0.155	0.0660	1.7690	2.2090	0.0000	2.4312	0.1	25.0	300
200	PCO2_09	0.357	0.1177	2.6560	3.6050	0.0000	4.0806	0.1	25.0	300
125	TEMP_03a	0.159	0.0656	1.7640	2.2100	0.0000	2.4363	0.5	52.5	300
125	TEMP_04a	0.153	0.0678	1.7740	2.2140	0.0000	2.4366	0.5	80.0	300
125	Ca_01a	0.041	0.0705	2.2220	2.4340	0.0000	2.5549	0.5	25.0	300
125	Ca_02a	0.358	0.0626	1.2200	2.0570	0.0000	2.4815	0.5	25.0	300
125	I_01a	0.152	0.0701	0.2504	0.6903	0.0000	0.9172	0.5	25.0	300
125	I_02a	0.161	0.0743	3.3700	3.8370	0.0000	4.0763	0.5	25.0	300
125	Mg_01a	0.164	0.0172	1.9740	2.3320	0.0000	2.5165	0.5	25.0	300
125	Mg_02a	0.158	0.1235	1.6870	2.2460	0.0000	2.5307	0.5	25.0	300
50	SO4_01a	0.040	0.0237	0.7296	0.8215	0.0115	0.9303	1.0	25.0	300
125	SO4_02a	0.154	0.0772	1.7770	2.2090	0.0117	2.4816	1.0	25.0	300
200	SO4_03a	0.345	0.1292	2.6300	3.5490	0.0127	4.0656	1.0	25.0	300

For each experiment concentration (molal), gas composition is X_{CO_2}, temperature (°C) and reactor stirring rate (RPM) are given. The gas mixture was balanced with nitrogen.

[a] $X_{CO_2} = 1 - \frac{CO_2,\ L\ min^{-1}}{CO_2+N_2,\ L\ min^{-1}}$.

$$\frac{dCaCO_3}{dt} = \frac{1}{2}\left(V\frac{dTA}{dt}\right), \tag{3}$$

where V is the mass of solvent since molal units are used. This requires that the pH–time data be converted to TA–time. The TA at time $= t$ can be calculated using EQPITZER by coupling pCO_2 (~constant) and pH at time $= t$.

A high order (7th-order) polynomial equation was necessary to fit the resulting TA–time data (Fig. 2) and accommodate the sharp hysteresis that occurs as the system nears equilibrium. A first derivative of the fitted equation was then used to calculate $\frac{dTA}{dt}$ and applied to Eq. (3). As a result of the poor asymptotic properties of high order polynomial equations, the $\frac{dTA}{dt}$ data had to be truncated near the terminus. The dissolution rates were then normalized to the available surface area. Given the high volume to surface area ratio (V:$A = 1.1$ cm) and small changes in alkalinity, no observable change in specific surface area was measured as evidenced from SEM imaging. Therefore, the available surface area was assumed to remain constant over the course of the dissolution.

Rate data were modeled using an empirical rate equation (see Morse and Arvidson, 2002, for discussion of application of different types of rate equations to calcite dissolution). The general rate equation is (e.g., Morse and Berner, 1972)

$$R = -\frac{dm_{calcite}}{dt} = k(1-\Omega)^n, \tag{4}$$

where R is the rate (mol m^{-2} h^{-1}), m is moles of calcite, t is time, k is the empirical rate constant and n is the reaction order. The equation describes the rate as a function of saturation state (Ω) with respect to calcite as defined simply as the ratio of the ion activity product (IAP) to the thermodynamic solubility constant (K_c), as given by

$$\Omega = \frac{IAP}{K_c} \tag{5}$$

and

$$IAP = \gamma_{Ca^{2+}} m_{Ca^{2+}} \gamma_{CO_3^{2-}} m_{CO_3^{2-}}, \tag{6}$$

where the carbonate ion concentration ($m_{CO_3^{2-}}$) and activity coefficients (γ) were calculated using EQPITZER. If $\Omega = 1$, then the solution is in equilibrium with respect to calcite; if $\Omega < 1$ the solution is undersaturated; and if $\Omega > 1$ the solution is supersaturated.

Gledhill and Morse (2004, in press) recently reported that, in brines >50 g L^{-1} TDS, the EQPITZER calculated IAP at steady-state systematically exceeds K_c at high calcium concentrations (i.e., >0.03 m). Consequently, calculated calcite saturation states may erroneously suggest in excess of a 2-fold supersaturation in the most concentrated brines. This was interpreted (Gledhill and Morse, in press) as being the result of a small uncertainty in the modeled carbonate ion activity coefficient. In these solutions, the carbonate ion occurs in very low concentration (<15 μmolal) and the predicted activity coefficient decreases to $\sim 3 \times 10^{-3}$ in the most concentrated brines. Jeschke and Dreybrodt (2002) showed that when rates are modeled as function of the degree of disequilibrium $(1-\Omega)$, small uncertainties in Ω can have a pronounced effect on the interpreted reaction order (n) and rate constant (k).

Table 2
Initial (i) and steady-state (ss) carbonic acid system parameters along with the final calcium concentrations (molal)

Experiment ID	Ca^{2+}_{ss}	pH_i	pH_{ss}	Electrode response (%)	TA_i (meq kg^{-1} H_2O)	TA_{ss} (meq $kg^{-1}H_2O$)	TCO_{2i} (molal)	TCO_{2ss} (molal)	pCO_2 (bar)
PCO2_01	0.042	5.655	5.820 ± 0.019	84	11.6	167 ± 0.1	0.0387	0.0432 ± 0.0012	0.98 ± 0.01
PCO2_02	0.158	5.312	5.624 ± 0.015	90	5.6	107 ± 0.0	0.0255	0.0301 ± 0.0004	0.89 ± 0.04
PCO2_03	0.348	5.064	5.427 ± 0.016	86	3.3	67 ± 0.2	0.0194	0.0222 ± 0.0001	0.92 ± 0.08
PCO2_04	0.042	5.823	6.039 ± 0.028	90	8.2	264 ± 0.1	0.0212	0.0264 ± 0.0005	0.45 ± 0.00
PCO2_05a	0.166	5.448	5.769 ± 0.006	94	4.0	80 ± 0.0	0.0143	0.0180 ± 0.0000	0.47 ± 0.01
PCO2_05b	0.157	5.448	5.769 ± 0.004	97	3.9	78 ± 0.1	0.0140	0.0178 ± 0.0001	0.46 ± 0.01
PCO2_05c	0.159	5.442	5.785 ± 0.010	91	3.9	80 ± 0.1	0.0145	0.0180 ± 0.0002	0.46 ± 0.02
PCO2_06	0.363	5.205	5.542 ± 0.005	97	3.4	46 ± 0.1	0.0115	0.0127 ± 0.0001	0.47 ± 0.02
PCO2_07	0.041	6.222	6.45 ± 0.002	85	3.9	61 ± 0.1	0.0063	0.0084 ± 0.0001	0.08 ± 0.00
PCO2_08	0.157	5.781	6.171 ± 0.010	69	1.7	35 ± 0.0	0.0038	0.0053 ± 0.0001	0.09 ± 0.01
PCO2_09	0.362	5.583	5.959 ± 0.005	83	1.0	22 ± 0.1	0.0026	0.0036 ± 0.0001	0.09 ± 0.01
TEMP_03a	0.151	5.431	5.754 ± 0.006	93	2.0	42 ± 0.0	0.0072	0.0094 ± 0.0001	0.37 ± 0.01
TEMP_04a	0.159	5.399	5.731 ± 0.003	99	1.2	24 ± 0.1	0.0048	0.0059 ± 0.0001	0.33 ± 0.01
Ca_01a	0.044	5.734	5.978 ± 0.003	87	7.8	127 ± 0.0	0.0177	0.0222 ± 0.0000	0.46 ± 0.03
Ca_02a	0.360	5.438	5.671 ± 0.002	93	3.6	60 ± 0.0	0.0142	0.0164 ± 0.0001	0.46 ± 0.01
I_01a	0.156	5.567	5.813 ± 0.001	86	4.7	81 ± 0.0	0.0188	0.0220 ± 0.0001	0.47 ± 0.01
I_02a	0.164	5.340	5.664 ± 0.008	88	3.1	59 ± 0.1	0.0105	0.0132 ± 0.0001	0.44 ± 0.03
Mg_01a	0.165	5.377	5.762 ± 0.006	98	3.3	76 ± 0.0	0.0134	0.0175 ± 0.0002	0.46 ± 0.02
Mg_02a	0.160	5.386	5.749 ± 0.004	92	3.4	75 ± 0.0	0.0137	0.0176 ± 0.0001	0.46 ± 0.02
SO4_01a	0.043	5.662	5.869 ± 0.004	90	11.2	179 ± 0.1	0.0365	0.0432 ± 0.0001	0.88 ± 0.00
SO4_02a	0.156	5.353	5.620 ± 0.002	90	5.9	105 ± 0.1	0.0252	0.0296 ± 0.0002	0.87 ± 0.03
SO4_03a	0.356	5.240	5.441 ± 0.007	90	4.4	66 ± 0.1	0.0191	0.0212 ± 0.0001	0.84 ± 0.04
PCO2_01b	0.043	5.642	5.894 ± 0.005	91	10.8	190 ± 0.1	0.0365	0.0445 ± 0.0002	0.89 ± 0.01
PCO2_01c	0.044	5.663	5.897 ± 0.004	90	11.4	189 ± 0.1	0.0374	0.0440 ± 0.0003	0.89 ± 0.02
PCO2_03b	0.363	5.074	5.457 ± 0.005	85	3.1	68 ± 0.1	0.0183	0.0216 ± 0.0002	0.86 ± 0.06
PCO2_03c	0.364	5.066	5.442 ± 0.011	87	3.1	66 ± 0.0	0.0184	0.0211 ± 0.0004	0.87 ± 0.07

Electrode response is reported as percent Nernstian. The pCO_2 was derived using EQPITZER from coupling TA and TCO_2 and the value reported is the mean of the initial and final conditions.

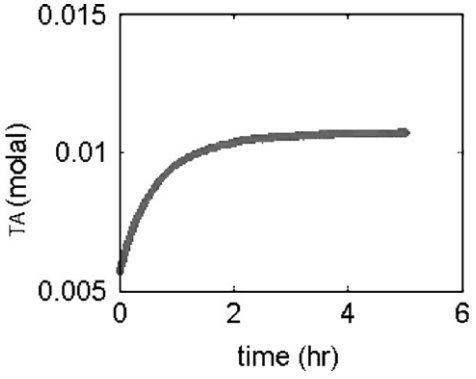

Fig. 2. The TA–time dependence of 2 g of calcite dissolved in a 0.5 L of 125 g L^{-1} 'model' brine at 25 °C and $X_{CO_2} = 1.0$. TA was calculated from pCO_2 (~constant) and pH measured every 5 s using EQPITZER.

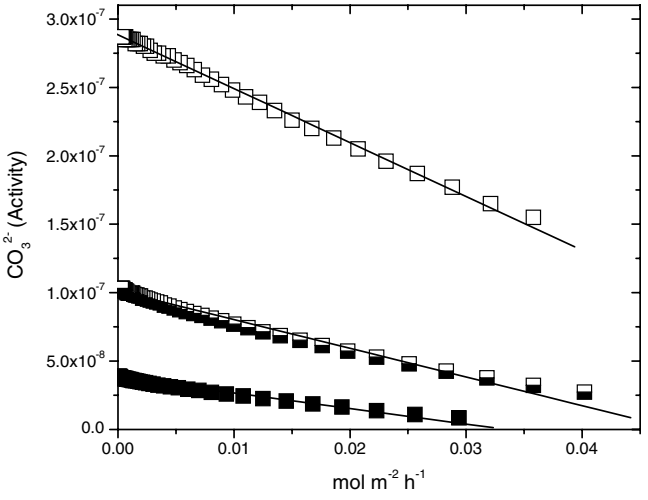

Fig. 3. The apparent carbonate ion activity, as calculated from the experimental data using EQPITZER, as a function of dissolution rate. Solid lines are linear least square regression fits of the experimental data. Dissolution in three 'model' brines with TDS concentrations of 50 (open square), 125 (half full square) and 200 (full square) g L^{-1} at 25 °C and $X_{CO_2} = 1.0$.

Therefore, given the small uncertainty associated with the EQPITZER carbonate ion activity, to model the rate data the Ω value in Eq. (4) was derived from an apparent steady-state solubility specific to each rate experiment.

4.2. Apparent steady-state solubility

Fig. 3 shows the change in carbonate ion activity as a function of dissolution rate for each of the 'model' brines. In all cases a near linear correlation was observed. The apparent steady-state carbonate ion activity ($a^*_{CO_3^{2-}}$) was estimated from the intercept of a linear least square regression (i.e., when the rate is zero; Table 3). Given that in these calcium-rich solutions the calcium activity remains nearly constant, the apparent saturation state (Ω^*) could be closely approximated by

Table 3
The apparent carbonate ion activity and ion activity product (IAP*) at equilibrium as extrapolated from rate data ($a^*_{CO_3^{2-}}$)

Experiment ID	$a^*_{CO_3^{2-}} \times 10^8$	IAP* $\times 10^9$	k	r^2
PCO2_01	28.8	2.61	72.8	1.00
PCO2_02	10.0	4.17	48.6	0.99
PCO2_03	3.7	5.09	33.9	0.99
PCO2_04	39.8	3.62	44.8	1.00
PCO2_05a	9.8	4.46	27.4	0.99
PCO2_05b	10.0	4.10	31.8	0.99
PCO2_05c	10.1	4.23	30.2	0.99
PCO2_06	3.4	5.28	22.8	0.99
PCO2_07	40.9	3.64	16.0	0.99
PCO2_08	11.4	4.75	12.0	0.99
PCO2_09	4.1	6.37	12.0	0.99
TEMP_03a	6.6	2.28	58.1	0.99
TEMP_04a	2.5	0.74	106.9	0.98
Ca_01a	25.8	3.53	25.3	0.98
Ca_02a	6.6	4.80	32.5	0.99
I_01a	13.8	3.71	43.7	0.99
I_02a	5.6	4.93	19.3	0.99
Mg_01a	9.7	4.52	30.0	0.99
Mg_02a	9.2	3.75	27.7	0.99
SO4_01a	34.4	3.09	49.6	0.99
SO4_02a	9.6	3.88	37.2	0.99
SO4_03a	3.5	4.98	22.8	0.98
PCO2_01b	38.0	4.03	85.7	0.99
PCO2_01c	37.6	3.51	32.8	0.99
PCO2_03b	3.8	0.12	44.2	0.99
PCO2_03c	3.9	5.74	12.3	0.93

The rate constant in mmol m^{-2} h^{-1} for the general rate equation in which $n = 1$.

$$\Omega^* = \frac{a_{Ca^{2+}} a_{CO_3^{2-}}}{K^*_{eq}} \approx \frac{a_{CO_3^{2-}}}{a^*_{CO_3^{2-}}}, \quad (7)$$

where K^*_{eq} is the apparent IAP at equilibrium (IAP*) calculated as the product of $a^*_{CO_3^{2-}}$ and the average steady-state calcium ion activity, which only varied a few percent from the mean value during experiments due to the generally relatively high calcium concentrations used. When modeled with respect to this apparent saturation state, first-order kinetics ($n = 1$) were sufficient to provide an excellent fit to the rate data. Reported in Table 3 are the k values (mmol m^{-2} h^{-1}) along with the correlation coefficients.

4.3. Calcite dissolution in 'model' brines

4.3.1. Effect of pCO_2

Dissolution rates measured in each of the 'model' brines at three CO_2 partial pressures ($X_{CO_2} = 1.0, 0.5$ and 0.1) are shown in Fig. 4 and their corresponding rate constants are plotted in Fig. 5 as a function of TDS. The EQPITZER calculated partial pressures as derived from TA and TCO_2 were 0.88 ± 0.04, 0.45 ± 0.01 and 0.08 ± 0.00 bar, respectively, reflecting the contribution of water vapor pressure.

Other investigators (e.g., Sjöberg, 1978; Busenberg and Plummer, 1986) have demonstrated a rate dependence on CO_2 for partial pressures above 0.1 bar and for pH values greater than about 4.5 when the rate is dominated by surface control reactions. Pokrovsky et al. (2005) found that, in the transport-controlled region far from equilibrium, solutions of up to 1 M NaCl also showed pCO_2 dependence. However, the dependence did not only persist beyond ~20 atm pCO_2. A strong pCO_2 dependence was observed in this study, where a 5-fold decrease in the rate constant was measured, when the partial pressure was

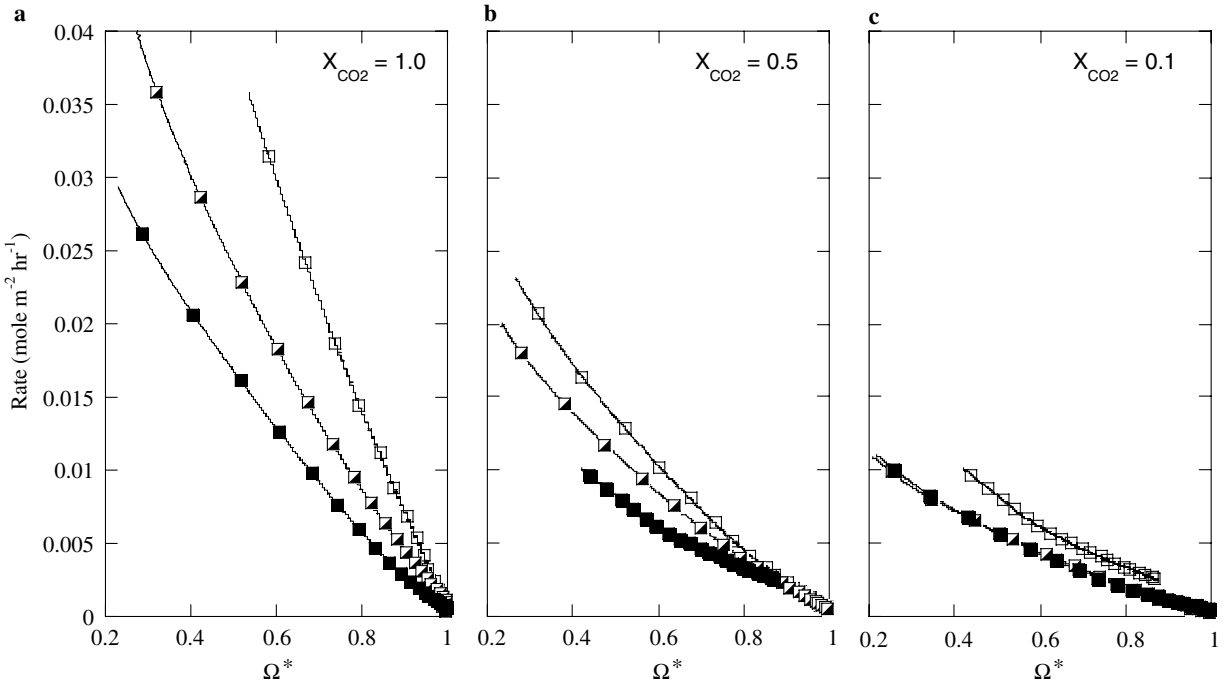

Fig. 4. The pCO_2 effect on rates of calcite dissolution in three 'model' brines with TDS concentrations of 50 (open square), 125 (half full square) and 200 (full square) g L^{-1} at 25 °C, where $X_{CO_2} = 1.0$ (a), 0.5 (b) and 0.1 (c).

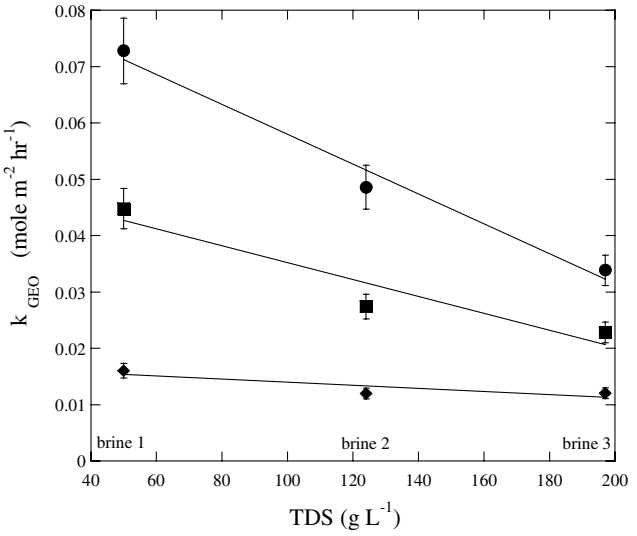

Fig. 5. The rate constant (k) as a function of TDS (g L^{-1}). In general, as brine TDS concentrations increase, the rates decrease, but this compositional effect is dependent on pCO_2. $X_{CO_2} = 1.0$ (solid circle), 0.5 (solid square) and 0.1 (solid diamond). Error bars represent analytical uncertainty.

reduced from 1 to approximately 0.1 bar (Fig. 5). Van Cappellen et al. (1993) attributed this CO_2 dependence to the formation of carbonate complexes with surface lattice calcium ions. According to their surface complexation model, the CO_2-promoted dissolution rate is directly proportional to the concentration of $>CaHCO_3^0$ sites (where $>$ represents the mineral lattice) and is an example of ligand promoted dissolution in which the formation of the bicarbonate surface complex increases the rate of detachment of Ca^{2+} from surface positions.

The inhibitory effects of the salts also appear to exhibit CO_2 dependence. Rates become progressively more depressed with increasing brine concentration but the effect is more pronounced at the higher partial pressures and all but absent at 0.1 bar.

4.3.2. Specific effects of Ca^{2+}, Mg^{2+} and ionic strength

The independent effects of Ca^{2+}, Mg^{2+} and ionic strength were investigated by measuring the dissolution rate in solutions that were modifications of the 125 g L^{-1} 'model' brine. In each case, one factor was varied while all other variables were held constant. For example, in the case of the Ca^{2+} effect experiments, two brines were prepared with Mg^{2+} concentration and ionic strength equivalent to the 125 g L^{-1} 'model' brine, but with Ca^{2+} concentrations equivalent to the 50 g L^{-1} 'model' brine (Experiment Ca_01a) and the 200 g L^{-1} 'model' brine (Experiment Ca_02a) respectively (Table 1). The experiments were performed under a $X_{CO_2} = 0.5$ atm at 25 °C and the rates compared against experiment PCO2_05a. By using this approach, the specific contribution to the net inhibition observed with increasing TDS (Figs. 4 and 5) could be evaluated.

An interesting finding was that the greatest inhibition to the rate was attributed to increasing ionic strength (Fig. 6a). Relatively few studies have examined the specific effect of ionic strength on calcite dissolution rates. Buhmann and Dreybrodt (1987) found that ionic strength was only of minor importance, but the study investigated very dilute solutions (<2 mM) compared with those studied here. Similarly, Pokrovsky et al. (2005) found that the rates, in the transport-controlled region far from equilibrium, did not depend on ionic strength for NaCl solutions of

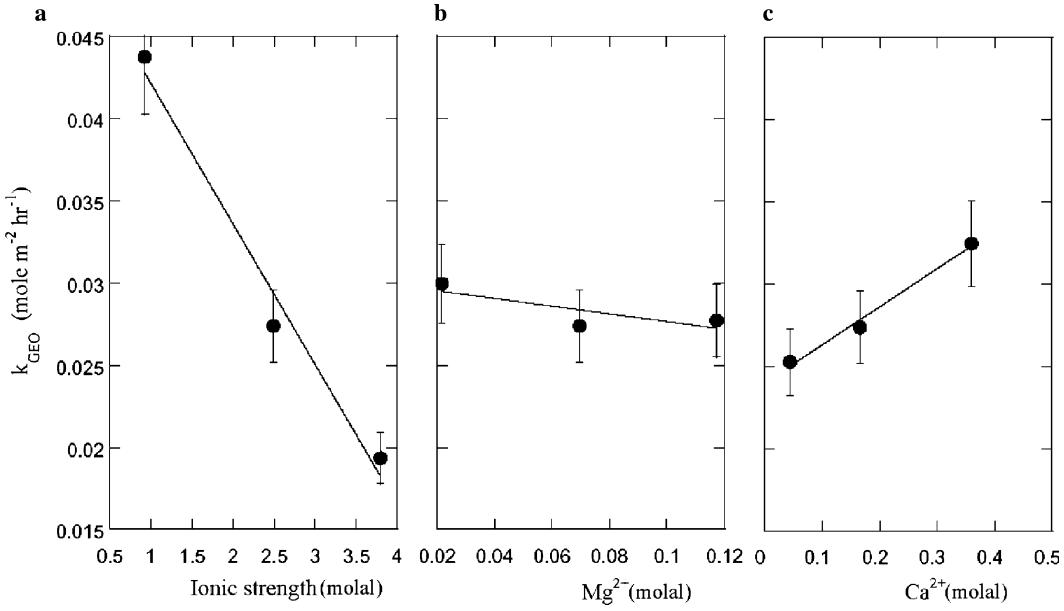

Fig. 6. The specific effects of ionic strength, Mg^{2+} and Ca^{2+} concentrations. The rate constant (k) (mol m^{-2} h^{-1}) as a function of the molal concentration of Ca^{2+} (a), Mg^{2+} (b) and ionic strength (c).

up to 1 M. In contrast, Zhang and Dawe (1998) found that, in high salinity waters (up to 2 mol kg^{-1}), the calcite precipitation rate increased as a function of the square root of ionic strength. Similarly, Bischoff (1968) found that nucleation rates of calcite also increased proportionally to the square root of ionic strength. Zuddas and Mucci (1998), in an extensive study of the influence of ionic strength on calcite precipitation from seawater, found the partial reaction order with respect to the carbonate ion concentration increased with ionic strength as did the forward reaction rate constant. It was suggested in these studies that with increased electrolyte concentrations, a stronger inter-particle attraction helps to catalyze calcite growth in a manner analogous to colloid flocculation. Such processes may conversely inhibit dissolution.

An alternative, though more speculative, explanation first put forth by Sjöberg (1978) that could account for both the increase precipitation rates observed in the prior studies, and the decreased dissolution rates measured in this study, is related to the effect of water activity on the hydration of metal ions. Lippmann (1973) and Arvidson and Mackenzie (1999) proposed the dehydration of cations poses a fundamental energetic barrier to precipitation. Conversely, the hydration of the calcium ion may pose an energetic barrier to dissolution. In order for calcite to dissolve, the attractive interaction of water molecules must overcome the ionic attraction within the mineral lattice. If, as a result of high ionic strength, the water activity is significantly diminished, one would expect the hydration efficiency of the calcium ion to be retarded. The rate constants shown in Fig. 6a change in a close to linear manner, in excess of a factor of two, over the range water activity in these experiments.

There have been a considerable number of investigations on the effects of magnesium ions on calcite dissolution (Berner, 1967; Weyl, 1967; Sjöberg, 1978; Buhmann and Dreybrodt, 1987; Compton and Brown, 1994; Gutjahr et al., 1996b; Alkattan et al., 2002). Whereas the magnesium ion has clearly been shown to strongly inhibit the rate of dissolution in neutral to basic solutions (e.g., Compton and Brown, 1994; pH 8–9), in acidic solutions the inhibition is absent (Alkattan et al., 2002; pH 1–3). At intermediate pH, such as in this study, the findings are often contradictory. Both Buhmann and Dreybrodt (1987) and Sjöberg (1978) report a strong inhibitory effect whereas Gutjahr et al. (1996b) found no effect.

In this study, only a modest inhibition was observed when magnesium was varied between 0.02 and 0.12 molal (Fig. 6b). Sjöberg (1978) described the inhibition due to magnesium in solutions containing <50 mM Mg^{2+} in terms of a Langmuir-type adsorption isotherm. The Langmuir–Volmer model would predict that, beyond some inhibitor solution concentration, the dissolution rate would become independent of the inhibitor concentration. It is possible that the absence of a strong effect in this study reflects that the magnesium concentrations of these brines have exceeded this inhibition plateau. Although Compton and Brown (1994) did measure an inhibition effect in solutions containing up to 80 mM Mg^{2+}, the pH of their experimental solutions was greater than 8, which may be above the pH of zero surface charge ($pH_{zpc} \approx 8.2$) (e.g., Hohl et al., 1980). Below the pH_{zpc} the effects of cationic inhibitors may be greatly diminished (Van Cappellen et al., 1993; Pokrovsky and Schott, 2002).

Several studies have also investigated the effect of the calcium ion on calcite dissolution (Sjöberg, 1978; Sjöberg and Rickard, 1985; Buhmann and Dreybrodt, 1987; Gutjahr et al., 1996a,b), often with contradictory results. Sjöberg (1978) found that increasing the Ca^{2+} concentration from 0 to 10 mM resulted in about a 17% decrease to the rate constant that he described in terms of a Langmuir-type adsorption isotherm similar to that of magnesium. In contrast, Gutjahr et al. (1996b) found that the rate constant actually increased by roughly 40% when Ca^{2+} concentrations were increased from 0.160 to 4.090 mM. The cause of the disparity between the different studies is unclear since amongst these studies the pH, pCO_2 and degree of disequilibrium are relatively similar.

In this study an increase in the measured rate constant was observed when calcium was increased from 0.04 to 0.36 molal (Fig. 6c). The experimental conditions of the previous studies, however, do differ considerably from this study, which was performed in moderately acidic pH (i.e., <6.5), high pCO_2 and magnesium-bearing solutions.

An important consideration is the effect that calcium has on the carbonate carrying capacity of the solution (e.g., Morse and Mackenzie, 1993). For a given degree of undersaturation, the relative amount of carbonate ion in solution is reduced when the initial calcium concentration is increased. The inhibiting effect CO_3^{2-} of has been demonstrated for dissolution far from equilibrium in the case of $ZnCO_3$ and $MnCO_3$ (Pokrovsky and Schott, 2002), dolomite and magnesite (Pokrovsky et al., 1999; Pokrovsky and Schott, 1999), and calcite (Lea et al., 2001; Arvidson, personal communication). Whether such inhibition effects occur near equilibrium or at this low CO_3^{2-} concentration has not yet been established, but they might contribute to the positive correlation between calcium and the rate constant measured here.

4.3.3. Temperature and stirring rate dependence

Temperature is one of the most important variables when considering reaction rate constants. Drastic variations in rates can occur owing to the exponential dependence of reaction rate on temperature, which is often assumed to follow the classic Arrhenius equation:

$$k = Ae^{-\left(\frac{E_a}{RT}\right)} \tag{8}$$

where A is the pre-exponential factor, E_a is the activation energy, R is the gas constant (8.314×10^{-3} kJ mol^{-1} K^{-1}) and T is the temperature in degrees Kelvin. The apparent activation energy for the dissolution reaction can be calculated from the slope of a plot of $\log k$ versus the reciprocal absolute temperature since

$$\ln k = \left(\frac{-E_a}{RT}\right) + \ln A. \quad (9)$$

A plot of $\ln k$ against $1/T$ for dissolution experiments performed using the 125 g L^{-1} 'model' brine conducted under a $X_{CO_2} = 0.5$ atm at 25.0, 52.5 and 82.5 °C is shown in Fig. 7. The apparent activation energy is calculated to be 21 ± 1 kJ mol^{-1} for this reaction. There are a wide range of activation energies reported for calcite dissolution (about 8–60 kJ mol^{-1}; see Morse and Arvidson, 2002 for review). In dilute solutions far from equilibrium where diffusion-controlled processes dominate, most reported values are close to 10 kJ mol^{-1} (e.g., Plummer et al., 1978; Sjöberg, 1978; Salem, 1994). However, larger values are believed to be typical of surface-controlled processes (Lasaga, 1998). The value determined in this study is in excellent agreement with the $E_a = 19 \pm 4$ kJ mol^{-1} reported by Alkattan et al. (1998).

As further evidence of surface-controlled kinetics, when experiment PCO2_05 (i.e., 125 g L^{-1} TDS, $X_{CO_2} = 0.5$, 25.0 °C) was replicated at 500 and 700 rpm, the rates varied by less than 8%, probably within experimental error when compositional effects among the replicates are considered. This stirring rate independence is consistent with surface-controlled dissolution.

4.4. Multiple regression analysis of the dependence of k on Ca^{2+}, Mg^{2+}, ionic strength, temperature and pCO_2

The kinetics of calcite dissolution have typically been described in terms of empirical or semi-empirical rate equations (e.g., Morse, 1978; Sjöberg, 1978; Busenberg and Plummer, 1986), classical chemical kinetics (e.g., Plummer et al., 1978) or surface speciation (Van Cappellen et al., 1993; Arakaki and Mucci, 1995; Pokrovsky and Schott, 2002) models. With the exception of some empirical models applied to seawater, these models are only applicable to relatively dilute solutions since accurately quantifying many of the required species (e.g., surface complexes) in concentrated solutions (i.e., >1 m) is beyond current geochemical models.

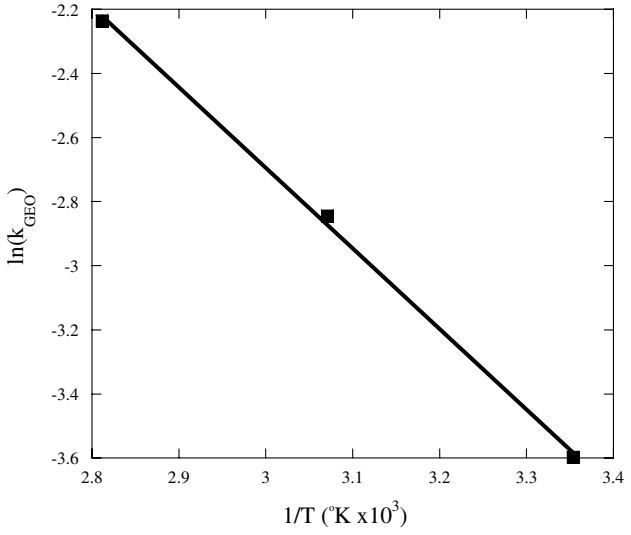

Fig. 7. Arrhenius plot for rates measured in the 125 g L^{-1} 'model' brine under a $X_{CO_2} = 0.5$ atm at 25.0, 52.5 and 82.5 °C. The apparent activation energy is 20.9 kJ mol^{-1} indicating a surface-controlled reaction.

A disadvantage of the general rate equation ($R = k(1 - \Omega)^n$) is that it requires fitting parameters (k and n) specific to the solution composition of interest, where the major solute and inhibitor concentrations and environmental conditions (e.g., P, T and pCO_2) are known. The first-order kinetics observed in this study across a broad range of typical brine concentrations requires that only one term, k, be determined. This greatly simplifies the approach since conventional statistical methods can be applied to account for the variably in k as a function of the key factors investigated.

A multiple regression analysis was used to evaluate to what extent the observed rate constant is dependent on each of the variables Ca^{2+}, Mg^{2+}, ionic strength, temperature and pCO_2. As with other regression models, multiple regressions (MR) may not be capable of yielding specific reaction mechanisms, but can estimate the relative strength of individual effects and, thus, be used to provide a predictive statistically based empirical rate equation. The goal of this approach is to fully describe the observed rate data as a function of each of the investigated factors.

The MR analysis was performed using the statistical software SPSS® v. 11.0 for Windows. The robustness of the model was evaluated from the coefficient of multiple determination (R^2) and by examination of the residuals. In addition, a colinearity diagnostic was determined. Colinearity is a common complication in MR that can occur when the effect of one independent variable on the dependent variable is contingent on the value of another independent variable (Philippi, 1993).

The greatest predictive capability (adjusted $R^2 = 0.953$, $P < 0.001$) was achieved when the data were left untransformed (i.e., linear regression) and activity was modeled rather than concentration in the cases of calcium and magnesium. The resulting regression yielded:

$$k = \beta_0 + \beta_1(t) + \beta_2(pCO_2) + \beta_3(I) + \beta_4(a_{Ca^{2+}}) + \beta_5\left(a_{Mg^{2+}}\right) \quad (10)$$

where t is °C, pCO_2 is given in bars, I is ionic strength and a_i are activities of calcium and magnesium. The unstandardized coefficients are provided in Table 4 for solving

Table 4
The coefficients derived from multiple regression analysis. These can be used to predict the rate constant from the predictors T °C, pCO_2, I, $a_{Ca^{2+}}$ and $a_{Mg^{2+}}$

Predictor	Coefficient	Unstandardized × 10^3	Standardized × 10^3
Constant	β_0	−6.07	
t (°C)	β_1	1.42	0.879
pCO_2 (bar)	β_2	48.56	0.499
I (molal)	β_3	−10.97	−0.475
$a_{Ca^{2+}}$	β_4	127.45	0.259
$a_{Mg^{2+}}$	β_5	−58.54	−0.059

the surface area normalized rate constant (k). The calculated condition numbers for colinearity for each of the predictors were less than 20 and the variance inflation factors (VIF) less than 10, indicating that severe colinearity was not a factor (Freund and Littell, 1986; Chatterjee and Price, 1991). Since the predictors used in the model are measured in different units, the standardized coefficients (Table 4) are required to compare the relative effects of each of the predictors. The relative effects are $t \gg pCO_2 \approx I > a_{Ca^{2+}} \gg a_{Mg^{2+}}$. The results show that the ionic strength strongly correlates with a reduction in rate, and that the inhibitory effect of magnesium is small in these solutions. It also reveals that the calcium activity is positively correlated with the dissolution rate. Fig. 8 illustrates the predictive capability of the model where the measured rate constants are plotted versus their predicted values.

When we compare the dissolution rates measured using powered calcite reported by Gledhill and Morse (2004) to those obtained using crushed rhombs, there are apparent gross dissimilarities. Specifically, although the powder rates generally decreased with increasing brine concentration, the net inhibition was relatively minor. In contrast, the crushed rhomb experiments reveal a stronger compositional effect at the same higher partial pressures. However, Fig. 8 reveals that the MR model closely predicts the rates constants of the powdered calcite. It suggests that the limited inhibition observed by Gledhill and Morse (2004) using powered calcite experiments is an artifact of the brine preparations. The median Ca:I ratio in the Gledhill and Morse (2004) experimental brines were about twice that of these experiments. Since the effects of calcium and ionic strength are inversely correlated, the subdued compositional inhibition observed in the powdered calcite experiments can be accounted for as a result of the calcium effect partially compensating for the inhibitory effect associated with ionic strength.

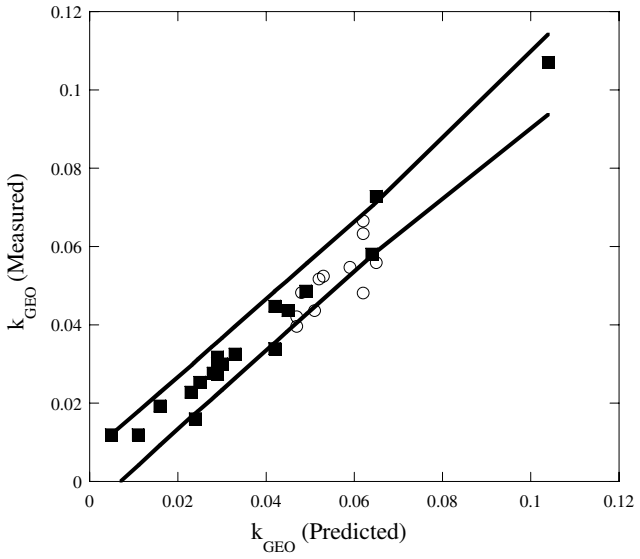

Fig. 8. The measured rate constants versus the predicted values from Eq. (10). The lines represent the 95% confidence interval of the model prediction. The regression was fit to data obtained from dissolution rates using the rhombic calcite (solid square). The statistical model closely predicts previously measured rates obtained using powdered calcite (Gledhill and Morse, 2004) (open circle).

4.5. The inhibitory effect of SO_4^{2-} in concentrated brines

A common inhibitor of calcite reaction (dissolution/precipitation) kinetics in natural waters is the divalent anion sulfate (Akin and Lagerwerff, 1965; Sjöberg, 1978; Buhmann and Dreybrodt, 1987; Mucci et al., 1989). Sulfate present at seawater concentration has been demonstrated to reduce the dissolution rate constant by 40% in phosphate-free pseudo seawater (Sjöberg, 1978). In subsurface formation waters sulfate is often, but not always, a relatively minor component rarely exceeding 1 g L^{-1} compared with 2.7 g L^{-1} in seawater. Nevertheless, Sjöberg (1978) found that the effect of sulfate increases with increasing calcium and magnesium concentration and, thus, it could potentially be an even more potent inhibitor in brines. This could be related to the surface adsorption of calcium and magnesium, producing a more cationic surface that increases the adsorption of anions such as sulfate.

To test the effect, approximately 1 g L^{-1} (~0.01 m) of sulfate was added to each of the 'model' brines in the form of a concentrated Na_2SO_4 solution. The dissolution rates were measured in each solution at 25 °C and $X_{CO_2} = 1$ and compared with its MR-model predicted rate. The higher CO_2 partial pressure was chosen since brines exhibited the greatest compositional sensitivity at this pCO_2. Fig. 9 shows the increasing inhibitory effect of sulfate with increasing calcium and magnesium activity, consistent with Sjöberg's (1978) findings. The equation fit to the data is purely an empirical construct, but does suggest that in the absence of calcium and magnesium the inhibitory effect

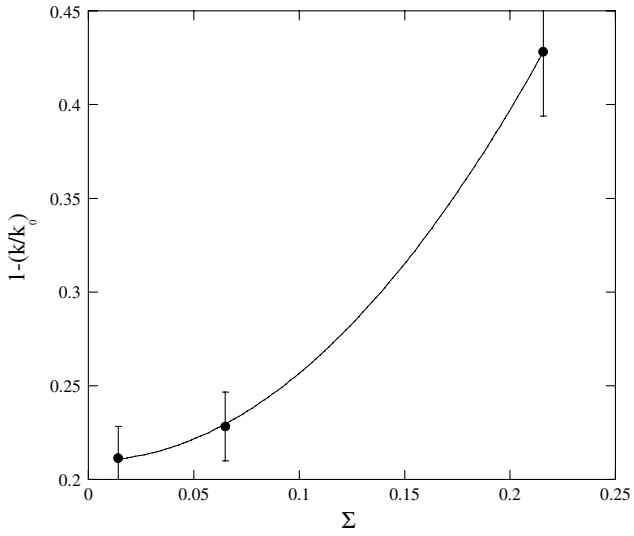

Fig. 9. The inhibitory effect of 1 g L^{-1} sulfate in 'model' brines at 25 °C at $X_{CO_2} = 1.0$. The measured rate constant (k) relative to the MR-model prediction (k_0) show that with increasing calcium and magnesium activity ($\sum = a_{Ca^{2+}} + a_{Mg^{2+}}$) the sensitivity to sulfate increases. The equation of the line shown is: $1 - (k/k_0) = 0.20 + 4.68(a^2_{Ca^{2+}} + a^2_{Mg^{2+}})$, $r^2 > 0.99$.

of 1 g L^{-1} SO_4^{2-} would only be about 20%. In brines containing a TDS of 200 g L^{-1} the inhibition could be similar to that observed in seawater.

5. Conclusion

The calcite dissolution rate near equilibrium ($\Omega > 0.2$) in concentrated Na–Ca–Mg–Cl brines, equivalent to subsurface formation waters ranging from TDS 50–200 g L^{-1}, were measured. The rates can be described using first-order kinetics by the general rate equation: $R = k(1 - \Omega)^n$, where $n = 1$ (first-order) and the rate constant k can be derived from the MR model:

$$k = \beta_0 + \beta_1(t) + \beta_2(\mathrm{pCO_2}) + \beta_3(I) + \beta_4(a_{\mathrm{Ca}^{2+}}) + \beta_5\left(a_{\mathrm{Mg}^{2+}}\right).$$

The strongest influence on the rate is not salt content but temperature and CO_2 partial pressure. Surprisingly, ionic strength strongly correlates with an inhibition of rate of dissolution beyond the specific effects of calcium and magnesium. Magnesium showed only a minor inhibitory effect whereas increasing calcium actually increased the rate constant.

When SO_4^{2-} is present at concentrations typical of subsurface formation waters there is a strong inhibition effect similar to that observed previously in seawater. The influence of sulfate is also strongly sensitive to the concentrations of calcium and magnesium. Due to this relation, even though sulfate concentrations in subsurface formation waters are generally less than that in seawater, at TDS concentrations greater than 200 g L^{-1}, its effect on the rate may be of similar magnitude. It should be noted that these results are applicable to relatively high pCO_2 (>0.1 atm) waters where the pH is $<\sim$6.5 and they should be extrapolated with considerable caution to waters of lower pCO_2 and higher pH values as is typical of sediment pore waters.

Acknowledgments

We offer a special thanks to Dr. Rolf Ardvidson of Rice University who has been invaluable, providing practical aid in terms of the BET measurements and useful theoretical discussions. Dr. Andreas Lüttge was kind enough to allow us access to his laboratory and surface area analytical system. Dr. W. Dreybrodt and an anonymous reviewer, as well as the handling Associate Editor A. Mucci, offered many insightful suggestions that improved this paper. This research was supported by the U.S. Department of Energy Grant DE-FG03-00ER-15033.

Associate editor: Alfonso Mucci

References

Akin, G.W., Lagerwerff, J.V., 1965. Calcium carbonate equilibria in solutions open to the air. II. Enhanced solubility of $CaCO_3$ in the presence of Mg^{2+} and SO_4^{2-}. *Geochim. Cosmochim. Acta* **29**, 353–360.

Alkattan, M., Oelkers, E.H., Dandurand, J.-L., Schott, J., 1998. An experimental study of calcite and limestone dissolution rates as a function of pH from −1 to 3 and temperature from 25 to 80° C. *Chem. Geol.* **151**, 199–214.

Alkattan, M., Oelkers, E.H., Dandurand, J.-L., Schott, J., 2002. An experimental study of calcite dissolution rates at acidic conditions and 25 °C in the presence of $NaPO_3$ and $MgCl_2$. *Chem. Geol.* **190**, 291–302.

Arakaki, T., Mucci, A., 1995. A continuous and mechanistic representation of calcite reaction-controlled kinetics in dilute solutions at 25 °C and 1 atm total pressure. *Aquat. Geochem.* **1**, 105–130.

Arvidson, R.S., Mackenzie, F.T., 1999. The dolomite problem: The control of precipitation kinetics by temperature and saturation state. *Am. J. Sci.* **299**, 257–288.

Berner, R.A., 1967. Comparative dissolution characteristics of carbonate minerals in the presence and absence of aqueous magnesium ion. *Am. J. Sci.* **265**, 45–70.

Bischoff, J.L., 1968. Kinetics of calcite nucleation: magnesium ion inhibition and ionic strength catalysis. *J. Geophys. Res.* **73**, 3315–3322.

Buhmann, D., Dreybrodt, W., 1987. Calcite dissolution kinetics in the system H_2O–CO_2–$CaCO_3$ with participation of foreign ions. *Chem. Geol.* **64**, 89–102.

Busenberg, E., Plummer, L.N. 1986. A comparative study of the dissolution and crystal growth kinetics of calcite and aragonite. In: Mumpton, F.A. (Ed.), Studies in Diagenesis., U.S. Geol. Surv. Bull. 1578, 99, pp. 139–168.

Case, L.C., 1945. Exceptional Silurian brine near Bay City, Michigan. *Am. Assoc. Petrol. Geol. Bull.* **29**, 567–570.

Chatterjee, S., Price, B., 1991. *Regression Analysis by Example*. Wiley, New York.

Compton, R.G., Brown, C.A., 1994. The inhibition of calcite dissolution/precipitation: Mg^{2+} cations. *J. Colloid Interface Sci.* **165**, 445–449.

Dickson, A.G., Goyet, C. (Eds.), 1994. Handbook of Methods for the Analysis of the Various Parameters of the Carbon Dioxide System in Sea Water. DOE v. 2, ORNL/CDIAC-74.

Freund, R.J., Littell, R.C., 1986. *SAS System for Regression*. SAS Institute Inc., Cary, NC.

Gledhill, D.K., Morse, J.W., 2004. Dissolution kinetics of calcite in NaCl–$CaCl_2$–$MgCl_2$ Brines at 25 °C and 1 bar pCO_2. *Aquat. Geochem.* **10**, 171–190.

Gledhill, D.K. Morse, J.W., in press. Calcite solubility in NaCl–$CaCl_2$–$MgCl_2$ brines. *Chem. Geol.*

Gran, G., 1952. Determination of the equivalence point in potentiometric titrations. *Part II. Analyst* **77**, 661–671.

Gutjahr, A., Dabringhaus, H., Lacmann, R., 1996a. Studies of the growth and dissolution kinetics of the $CaCO_3$ polymorphs calcite and aragonite I. Growth and dissolution rates in water. *J. Cryst. Growth* **158** (3), 296–309.

Gutjahr, A., Dabringhaus, H., Lacmann, R., 1996b. Studies of the growth and dissolution kinetics of the $CaCO_3$ polymorphs calcite and aragonite II. The influence of divalent cation additives on the growth and dissolution rates. *J. Cryst. Growth* **158**, 310–315.

Hanor, J.S. 1994a. Origin of saline fluids in sedimentary basins. In: Parnell, E.J. (Ed.), Geofluids: Origin, Migration, and Evolution of Fluids in Sedimentary Basins, Geol. Soc. Spec. Pub. 78, pp. 151–174.

Hanor, J.S., 1994b. Physical and chemical controls on the composition of waters in sedimentary basins. *Marine Petrol. Geol.* **11**, 31–45.

He, S., Morse, J.W., 1993. The carbonic acid system and calcite solubility in aqueous Na–K–Ca–Mg–Cl–SO_4 solutions from 0 to 90 °C. *Geochim. Cosmochim. Acta* **57**, 3533–3554.

Hohl, H., Sigg, L., Stumm, W. 1980. Characterization of surface chemical properties of oxides in natural waters. In: Kavanaugh, M.C., Leckie, J. O. (Eds.), Particulates in Water, vol. 189, pp. 1–31.

Jeschke, A.A., Dreybrodt, W., 2002. Pitfalls in the determination of empirical dissolution rate equations of minerals from experimental data and a way out: An iterative procedure to find valid rate equations, applied to Ca-carbonates and -sulphates. *Chem. Geol.* **192** (3-4), 183–194.

Lasaga, A.C., 1998. *Kinetic Theory in the Earth Sciences*. Princeton Universtity Press.

Lea, A.S., Amonette, J.E., Baer, D.R., Liang, Y., Colton, N.G., 2001. Microscopic effects of carbonate, manganese, and strontium ions on calcite dissolution. *Geochim. Cosmochim. Acta* **65**, 369–379.

Lippmann, F., 1973. *Sedimentary Carbonate Minerals*. Springer-Verlag, New York.

Morse, J.W., Berner, R.A., 1972. Dissolution kinetics of calcium carbonate in sea water. II. Kinetic origin for the lysocline. *Am. J. Sci.* **272**, 840–851.

Morse, J.W., 1978. Dissolution kinetics of calcium carbonate in seawater. VI: The near-equilibrium dissolution kinetics of calcium carbonate-rich deep sea sediments. *Am. J. Sci.* **278**, 344–353.

Morse, J.W., 1983. The kinetics of calcium carbonate dissolution and precipitation. In: Reeder, R.J. (Ed.), *Carbonates: Mineralogy and Chemistry*. Mineralogical Society of America, Washington, DC., pp. 227–264.

Morse, J.W., Mackenzie, F.T., 1990. *Geochemistry of Sedimentary Carbonates*. Elsevier, Amsterdam.

Morse, J.W., Mackenzie, F.T., 1993. Geochemical constraints on $CaCO_3$ transport in the subsurface. *Chem. Geol.* **105**, 181–196.

Morse, J.W., Arvidson, R.S., 2002. The dissolution kinetics of major sedimentary carbonate minerals. *Earth-Sci. Rev.* **58**, 51–84.

Mucci, A., Canuel, R., Zhong, S., 1989. The solubility of calcite and aragonite in sulfate-free seawater and the seeded growth kinetics and composition of the precipitates at 25 °C. *Chem. Geol.* **74**, 309–320.

Murphy, J., Riley, J.P., 1962. A modified single solution method for the determination of phosphate in natural waters. *Anal. Chim. Acta* **27**, 31–36.

Philippi, T.E., 1993. Multiple regression: Herbivory. In: Scheiner, S.M., Gurevitch, J. (Eds.), *Design and Analysis of Ecological Experiments*. Oxford University Press, Oxford, NY, pp. 183–210.

Plummer, L.N., Wigley, T.M.L., Parkhurst, D.L., 1978. The kinetics of calcite dissolution in CO_2–water systems at 5–60 °C and 0.0–1.0 atm CO_2. *Am. J. Sci.* **278**, 179–216.

Plummer, L.N., Parkhurst, D.L., Wigley, T.M.L., 1979. Critical review of the kinetics of calcite dissolution and precipitation. In: Jenne, E. (Ed.), *Chemical Modeling—Speciation, Sorption, Solubility and Kinetics in Aqueous Systems*. American Chemical Society, Washington, DC, pp. 537–573.

Pokrovsky, O.S., Schott, J., 1999. Processes at the magnesium-bearing carbonates/solution interface. II. Kinetics and mechanism of magnesite dissolution. *Geochim. Cosmochim. Acta* **63**, 881–897.

Pokrovsky, O.S., Schott, J., 2002. Surface chemistry and dissolution kinetics of divalent metal carbonates. *Environ. Sci. Technol.* **36**, 426–432.

Pokrovsky, O.S., Golubev, S.G., Schott, J., 2005. Dissolution of calcite, magnesite and dolomite at 25 °C and 0–50 atm pCO_2. *Chem. Geol.* **217**, 235–255.

Pokrovsky, O.S., Schott, J., Thomas, F., 1999. Dolomite surface speciation and reactivity in aquatic systems. *Geochim. Cosmochim. Acta* **63**, 3133–3143.

Salem, M.R., 1994. Dissolution of calcite crystals in the presence of some metal ions. *J. Mater. Sci.* **29**, 6463–6467.

Sjöberg, E.L., 1978. Kinetics and mechanism of calcite dissolutions in aqueous solutions at low temperature. *Stockholm Contr. Geology.* **32**, 1–96.

Sjöberg, E.L., Rickard, D., 1983. The influence of experimental design on the rate of calcite dissolution. *Geochim. Cosmochim. Acta* **47**, 2281–2285.

Sjöberg, E.L., Rickard, D.T., 1985. The effect of added dissolved calcium on calcite dissolution kinetics in aqueous solutions at 25[deg]C. *Chem. Geol.* **49** (4), 405–413.

Van Cappellen, P., Charlet, L., Stumm, W., Wersin, P., 1993. A surface complexation model of the carbonate mineral–aqueous solution interface. *Geochim. Cosmochim. Acta* **57**, 3505–3518.

Weyl, P.K., 1967. Solution behavior of carbonate materials in sea water. *Stud. Trop. Oceanogr.* **5**, 178–228.

Zhang, Y., Dawe, R., 1998. The kinetics of calcite precipitation from a high salinity water. *Appl. Geochem.* **13**, 177–184.

Zuddas, P., Mucci, A., 1998. Kinetics of calcite precipitation from seawater: II. The influence of ionic strength. *Geochim. Cosmochim. Acta* **62**, 757–766.